ELSEVIER

International Journal of Heat and Fluid Flow 19 (1998) 49–55

International Journal of HEAT AND FLUID FLOW

Finite element simulation of transient laminar flow and heat transfer past an in-line tube bank

Y.T. Krishne Gowda [a], B.S.V.P. Patnaik [b], P.A. Aswatha Narayana [b,*], K.N. Seetharamu [c]

[a] *Department of Mechanical Engineering, PES College of Engineering, Mandya 571401, India*
[b] *Department of Applied Mechanics, Indian Institute of Technology, Madras 600 036, India*
[c] *Department of Mechanical Engineering, Indian Institute of Technology, Madras 600 036, India*

Received 21 September 1996; accepted 14 June 1997

Abstract

Finite element simulation of transient laminar flow past an in-line tube bank is carried out using a velocity correction procedure. The two-dimensional unsteady Navier–Stokes and energy equations are solved using an explicit and a semi-implicit algorithm for a Reynolds number of 100, a Prandtl number of 0.7, and pitch-to-diameter ratios (PDR) of 1.5 and 2.0. The Galerkin weighted residual formulation is used for the discretization in space. Numerical flow visuals are drawn, showing the time evolution of streamlines. Local and average Nusselt numbers, pressure, and shear stress distributions around the cylinders have also been determined. The results compare well with existing numerical simulations.

Keywords: In-line tube bank; Explicit scheme; Heat exchangers; Finite element method; Semi-implicit scheme; Transient analysis

Notation

C_f	skin friction coefficient
C_p	pressure coefficient
D	diameter of the cylinder
h	heat transfer coefficient
k	thermal conductivity
Nu	Nusselt number (hD/K)
P	nondimensional pressure $(p/\rho U_{av}^2)$
Pe	Peclet number (Re*Pr)
Pr	Prandtl number $(\mu C_p/k)$
Re	Reynolds number $(U_{av}D/v)$
T	temperature
T_b	bulk temperature at minimum cross section
U	nondimensional axial velocity (u/U_{av})
V	nondimensional normal velocity (v/U_{av})
X	nondimensional axial coordinate (x/D)
Y	nondimensional normal coordinate (y/D)

Greek

θ	nondimensional temperature $(T - T_{in})/(T_w - T_{in})$
v	coefficient of kinematic viscosity
μ	coefficient of dynamic viscosity
ρ	density
τ	nondimensional time $(t^* U_{av}/D)$

Subscripts

av	average
w	wall
in	inlet

1. Introduction

Flow past tube banks with various configurations has wide ranging practical applications, such as in heat exchangers, nuclear reactors, boilers, condensers, waste heat recovery systems, cooling of electronic equipment, etc. An understanding of the wake behavior and the associated dynamics for flow past an array of tubes forms the first step for better design of the above-mentioned heat transfer equipment. Zukauskas (1987) has reviewed the experimental data of his group on forced convection past tube bundles.

The advent of modern high-speed computers has paved the way for the numerical solution of heat and momentum transfer problems in tubular heat exchangers. The first numerical investigations were reported by Launder and Massey (1978) for the tube bank problem. The numerical work of Fujii et al. (1984) made use of a finite-difference method. They used a one step forward and half a step backward iteration procedure, which is a hybrid technique to solve the stream function vorticity and energy equations for a five-row deep tube bank with 1.5×1.5 pitch-to-diameter ratio (PDR) and for Reynolds numbers up to 300. Dhaubhadel et al. (1986) presented a finite-element solution to the problem of steady flow across an in-line bundle of cylinders for Reynolds numbers up to 400

* Corresponding author. E-mail: hmtl@iitm.ernet.in.

0142-727X/98/$19.00
PII: S0142-727X(97)10005-4

and pitch-to-diameter ratios PDRs of 1.5 and 2.0. Wung and Chen (1989) made finite analytic calculation of convective heat transfer for in-line and staggered tube arrays in cross flow with Reynolds numbers ranging from 40 to 800 and PDR = 2.0. Numerical predictions of laminar and turbulent fluid flow and heat transfer around staggered and in-line tube banks in two and three dimensions were presented by Franz et al. (1995). However, in all these investigations, mostly steady-state results have been reported. To have a better insight, an analysis of the time evolution of flow over tube bundles is equally important, which is not now available in the literature.

Unsteady external flows with transients for convective heat transfer have recently received greater attention in connection with the increasingly greater use of automatic control devices for the accurate control of fluid flow in high-performance heat exchangers. Accurate regulation of fluid flow is of primary importance, when the positive control of these industrial devices must be ensured, which requires a better understanding and more precise evaluation of flow and thermal transients. This also has ramifications in the starting and shutting down phases of heat exchange.

In the present investigation, two algorithms (explicit and semi-implicit) have been implemented to solve the unsteady two-dimensional Navier–Stokes and energy equations. This study is primarily concerned with the transient fluid flow and thermal response of in-line tube banks, where emphasis is given to numerical flow visualization. The tube bank arrangement selected for the study is an in-line array with PDRs of 1.5 and 2.0. A Reynolds number of 100 and Prandtl number of 0.7 have been used. Time evaluation of streamlines, temperature contours, local and average Nusselt numbers, and pressure and shear-stress distributions around the cylinders are presented.

2. Formulation and numerical procedure

For two-dimensional flow of an incompressible fluid with negligible viscous dissipation, the dimensionless form of the Navier–Stokes and energy equations can be written as follows.

Continuity:

$$\frac{\partial U}{\partial X}+\frac{\partial V}{\partial Y}=0. \tag{1}$$

Momentum:

$$\frac{\partial U}{\partial \tau}+U\frac{\partial U}{\partial X}+V\frac{\partial U}{\partial Y}=-\frac{\partial P}{\partial X}+\frac{1}{\mathrm{Re}}\left(\frac{\partial^2 U}{\partial X^2}+\frac{\partial^2 U}{\partial Y^2}\right). \tag{2}$$

$$\frac{\partial V}{\partial \tau}+U\frac{\partial V}{\partial X}+V\frac{\partial V}{\partial Y}=-\frac{\partial P}{\partial Y}+\frac{1}{\mathrm{Re}}\left(\frac{\partial^2 V}{\partial X^2}+\frac{\partial^2 V}{\partial Y^2}\right). \tag{3}$$

Energy:

$$\frac{\partial \theta}{\partial \tau}+U\frac{\partial \theta}{\partial X}+V\frac{\partial \theta}{\partial Y}=\frac{1}{\mathrm{Pe}}\left(\frac{\partial^2 \theta}{\partial X^2}+\frac{\partial^2 \theta}{\partial Y^2}\right). \tag{4}$$

The solution algorithm employed in the present study is based on an Eulerian velocity correction method (Donea et al., 1982; Ramaswamy et al., 1992). In each time-step of the algorithm, the following four steps are repeated:

1. calculating intermediate velocities by ignoring the pressure term from the momentum equations;
2. evaluating for pressures from the pressure Poisson equation;
3. correcting the intermediate velocities; and
4. obtaining the temperatures from the energy equation.

The finite element spatial discretization is performed using linear triangular elements. The Galerkin-weighted residual method is used to formulate the spatial discretization. The procedural steps involved are given in an early study by Patnaik et al. (1996) while solving the problem of flow past a circular cylinder. The formulation is elaborated in detail in Krishne Gowda (1996).

3. Problem statement

3.1. Flow geometry

The physical model of flow around a five-row deep in-line tube bank is shown in Fig. 1. It is well established from the experimental flow visualizations of Braun and Kudriavtsev (1995) that the heat flux between the third and fourth row in a five-row bundle of cylinders is equivalent to the heat flux between any two adjacent inner rows of an infinite bundle of cylinders. For relatively low Reynolds numbers and closely packed cylinders, it is reasonable to assume that the wake of each cylinder is symmetric. In fact, no shedding is likely to occur, even at moderate Reynolds numbers, if the cylinders are tightly packed. It is assumed here that the symmetry lines exist as depicted in Fig. 1. The computational domain is shown by a thick dotted line. A close-up view of the finite element mesh is shown in Fig. 2. The grid is generated by an isoparametric mapping procedure. It is judiciously chosen and is very fine in the regions where the gradient fluxes are very high. Furthermore, the band width is reduced by implementing the Collins (1973) algorithm to exploit the storage space and the computing time involved. The inflow boundary is located at five cylinder diameters in front of the first row of cylinders. Similarly, in order to minimize the effects of the outflow boundary conditions on flow characteristics in the vicinity of the fifth cylinder, the computational mesh has been extended up to 15 cylinder diameters downstream of the fifth row of cylinders.

3.2. Boundary conditions

The following boundary conditions have been used for the computations:

a. cylinder surface: No slip ($U = V = 0.0$) and $\theta = 1.0$;
b. axis of symmetry: $V = 0.0$;
c. inlet: uniform flow and $\theta = 0.0$; and
d. exit: $P = 0.0$.

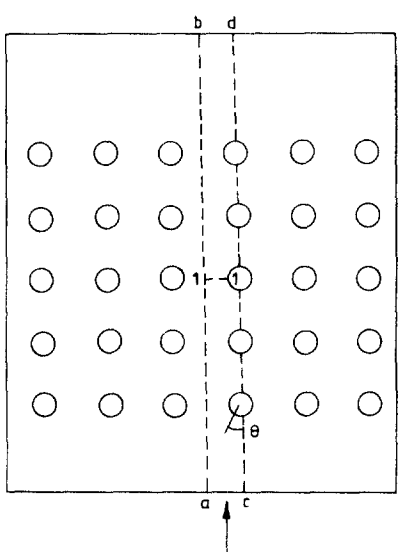

Fig. 1. Physical model.

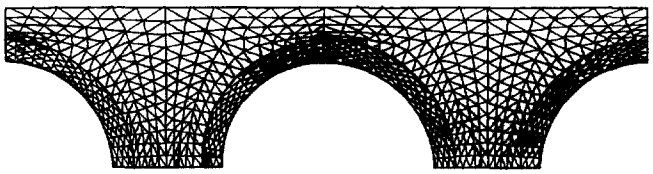

Fig. 2. Close-up view of finite element mesh.

3.3. Initial conditions

In the present investigation, the flow and thermal behavior during the starting phase of the heat exchange is of particular interest. Therefore, to closely simulate this behavior $\theta = 0, U = 0$, and $V = 0$ are specified everywhere at $\tau = 0$. For $\tau > 0$, the boundary conditions as specified above are imposed. The subsequent development of the flow and thermal fields are monitored.

3.4. Grid independence test

It is well known that the discretization process involves an error that can be reduced in principle, by grid refinement. The following three meshes are considered for the grid sensitivity analysis. The problem under consideration is an in-line tube bank with pitch to diameter ratio of 1.5:

(A) 1727 nodes; 3072 elements;
(B) 2539 nodes; 4608 elements; and
(C) 2945 nodes; 5376 elements.

In the present computations, mesh B has been arrived at as the optimum mesh. The computational results show a maximum difference of about 1.5% in the local and average Nusselt numbers between grids B and C. Also, the B mesh has been chosen for further analysis, because the results predicted from this mesh also agree well with the available results for steady flow past in-line tube bundles.

4. Comparison of explicit and semi-implicit schemes

Unlike the case of the explicit scheme, in the semi-implicit scheme, the intermediate velocity and the temperature fields are actually solved from the algebraic equations. This consumes considerable CPU time. In the case of an explicit scheme, mass lumping greatly simplifies the solution procedure and reduces it to merely an updating procedure. Thus, the time taken for each iteration in an explicit scheme is much less than that for a semi-implicit scheme. However, from stability considerations, the semi-implicit scheme allows a much larger time step and results in a reduction of the total CPU time compared with an explicit scheme.

Table 1 shows a comparison of the computational time required by the two numerical schemes for the case of flow over an in-line bundle of cylinders at Re = 100 and Pr = 0.7. The table clearly reveals that the semi-implicit scheme is about two times faster than the explicit scheme. Thus, the results of this comparison clearly weigh in favor of the semi-implicit scheme for the present investigation.

Table 1
Comparison of explicit and semi-implicit schemes on a PC486

Details	Explicit	Semi-implicit
Time required for 100 time steps	215 s	618 s
Total number of time steps	11,250	1500
Total time required to reach steady state	6.72 h	3.5 h

5. Results and discussion

Transient fluid flow and heat transfer past an in-line tube bank has been numerically simulated for PDRs of 1.5 and 2.0, Reynolds number of 100, and Prandtl number of 0.7.

5.1. Streamlines

The time evolution of streamlines for flow past tube banks is depicted in Fig. 3. The first instant when the flow comes into contact with the cylinders, its presence will not be felt by the flow. Hence, the inertia forces dominate the viscous forces. In the case of PDR = 1.5 and at $\tau = 0.1$ (Fig. 3(a)), the streamline pattern resembles that of an inviscid flow. The streamlines here show a fore and an aft symmetry as in the potential flow. Furthermore, the symmetry is lost at $\tau = 0.2$, except for the last row of cylinders, the incipience (the first time appearance) of separation can be seen on all the rows of cylinders, where the boundary layer separates. The eddy in which the fluid circulates keeps growing with time until it reaches steady state. The first reattachment of the eddy onto its downstream row of cylinders is seen at around $\tau = 0.5$. The size of the eddy between the cylinders grows with time and has reached maximum size at $\tau = 0.7$. This implies that the recirculatory eddy passes through a maximum before settling down to a steady-state value. The length of the recirculatory eddy behind the fifth row of cylinders increases with time, while the width of the eddy has reached a temporary maximum before reaching the steady state. It is observed from the plots that the time of separation and reattachment is also a function of PDR. However, for the sake of brevity, only the steady-state results are presented for PDR = 2.0 in Fig. 3(g).

5.2. Isotherms

Fig. 3 also shows the time evolution of isotherms. These portray the movement of heat flow at a given instant of time. In Fig. 3, it can be seen that, irrespective of the time, the isotherms are crowded over the front half of the first row of cylinders, indicating a high radial heat flux. In the upstream region of the first row of cylinders, this distribution is regular, packed, and remains uninfluenced, even after the steady state is reached. The isotherms at $\tau = 0.1$ of Fig. 3 are crowded over the entire cylinder and are symmetrical. As time passes, this symmetry is lost because of the recirculation region between the cylinders. The growth of isotherms follows that of the streamlines. Crowding of isotherms over the entire front half of the first row is understandable, because the thermal boundary layer growth begins from the first row. Over the other rows, low velocity recirculating flow interacts with parts of the front half of the subsequent cylinders. It is also seen from the plots that there is crowding of isotherms only over those regions where the flow has not separated.

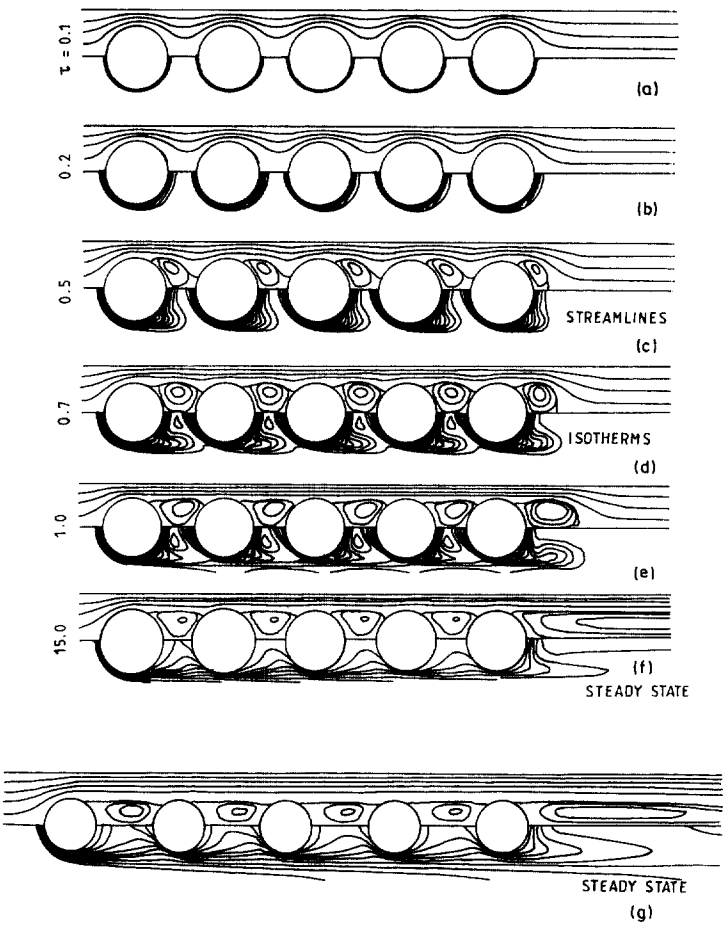

Fig. 3. Streamlines and isotherms for PDR = 1.5 and 2.0; streamline (ψ) values −0.020, −0.015, −0.010, −0.05, 0.0, 0.05, 0.10, 0.15, 0.20, and 0.25; isotherm (θ) values 0.1, 0.2, 0.3, 0.4, 0.5, 0.6, 0.7, 0.8, 0.9, and 1.0.

5.3. Skin friction coefficient

Shearing action between the fluid and the cylinder surface results in viscous friction, which is also known as skin friction. The local skin friction coefficient is defined by

$$C_f = \frac{2}{\mathrm{Re}} \frac{\partial U}{\partial Y}\bigg|_{Y=R}. \tag{5}$$

The time evolution of local skin friction coefficient around the cylinders is shown in Fig. 4(a) for PDR = 1.5. At $\tau = 0.1$, the distribution of skin friction coefficient is of the same form for all the rows of cylinders and for both the cases under investigation. This is because the flow initially behaves like a potential flow. The maximum local friction coefficient is the same for all the rows of cylinders. At $\tau = 1.0$, the skin friction distribution is almost the same for all the rows of cylinders except the front half of the first row and for the region over the rear half of the last row. The minimum value of C_f that is initially on the rear half of the cylinders has shifted to the front portion of the cylinders with progress in time. The negative maximum value for all the rows of cylinders (except the first row) can be seen at $\tau = 1.0$, and then it decreases by the time it reaches steady state. Comparison of local skin friction coefficients for the case of an in-line tube bank with PDR = 1.5 with Dhaubhadel et al. (1986) for the steady state is shown in Fig. 4(c). A good comparison can be seen. The steady-state distribution of friction coefficient is given in Fig. 4(b). As the PDR is increased to 2.0, the distribution of the local friction coefficient is found to be same, up to $\tau = 1.0$. The rate at which these values are decreasing is also the same for all the rows of cylinders. The values of local friction coefficients for all the rows of cylinders are less when compared to corresponding rows at PDR = 1.5. This is because the velocity gradients are lower at higher pitch to diameter ratios.

The variation of average friction coefficient up to $\tau = 0.1$ is found to be the same for all the rows of cylinders, but it is seen to be dependent on PDR. During the starting phase of the flow, there is a monotonic decrease in the values of average friction coefficients over all the rows of cylinders. The value of the average friction coefficient is greater for the first cylinder, as compared with the rest of the cylinders. Increasing the PDR to 2.0, the time taken for the average friction coefficient to reach a steady-state value is observed to be greater.

5.4. Nusselt number

Nusselt number is one of the vital parameters of interest to the designer. The local Nusselt number is defined by

$$\mathrm{Nu} = \frac{\theta_w - \theta_{in}}{\theta_w - \theta_b} \frac{\partial \theta}{\partial Y}\bigg|_{Y=R}. \tag{6}$$

Fig. 5 shows the distribution of local Nusselt numbers around the cylinders with time. In the initial phase, the distribution of local Nusselt number is almost the same on all the rows of cylinders and for both the cases under investigation.

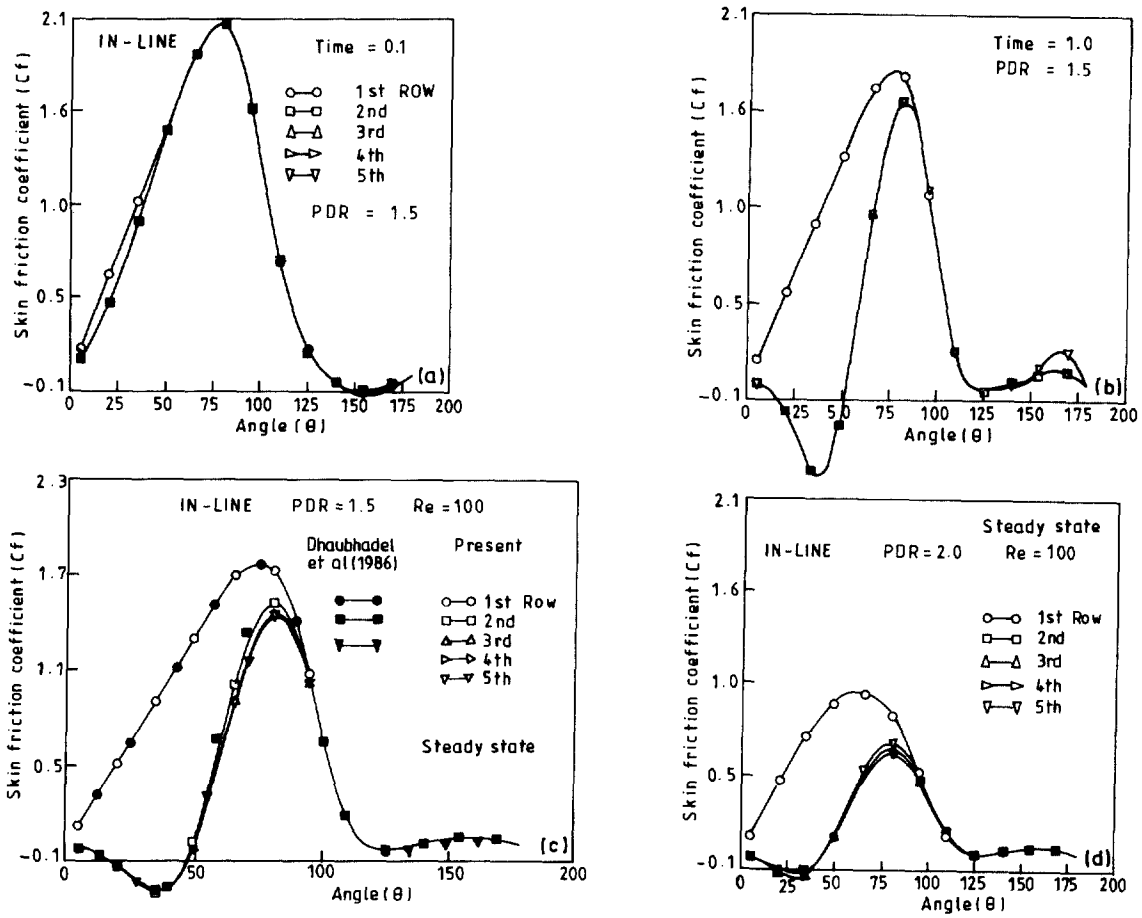

Fig. 4. Distribution of local friction coefficients: PDR = 1.5.

In the case of PDR = 1.5 and at $\tau = 0.1$ (Fig. 5(a)), the maximum local Nusselt number occurs at an angle of 50° over all the rows of cylinders. At $\tau = 0.5$, local Nusselt number value over the first row of cylinders is less, when compared to other rows of cylinders. It has been observed that for $\tau = 5.0$, the local Nu distribution in the range of 0–120° has almost stabilized for all the rows of cylinders except for the rear half of the fifth row. The size of the recirculation zone between the cylinders influences the local Nusselt number. This influence can further be seen in the form of higher local Nu values on the aft of the last row of cylinders. The plots indicate that the angle at which the maximum local Nu occurs has moved from 50° (at $\tau = 0.1$) to 60° (steady state). The steady state is reached around $\tau = 15.0$ (Fig. 5(c)). Here, it can also be noticed that the Nusselt number distribution for the first row differs from the second and subsequent rows. This happens as there is no "wake-shading" influence on the upstream of the first cylinder. As a result, the thinner boundary-layer over the first cylinder leads to a higher temperature gradient and, thus, higher heat transfer at the cylinder surface. For the local Nu distribution over the first cylinder, the minimum Nu in the plot corresponds to the boundary-layer separation point. The maximum Nu for the first row occurs at around 60°, which is in agreement with Fujii et al. (1984) and Dhaubhadel et al. (1986). A good agreement of local Nusselt number for the case of in-line tube bank for PDR = 1.5, with that of Dhaubhadel et al. (1986) can be seen for steady state. In the case of PDR = 2.0, the local distribution of Nu around the cylinder is found to be of the same form up to $\tau = 1.0$, unlike the case for PDR = 1.5. Only the steady-state results are presented for PDR = 2.0 in Fig. 5(d).

The variation of average Nusselt number with time for different rows of cylinders have been obtained. Up to $\tau = 0.1$, the value of the average Nusselt number is independent of PDR. In both the cases under investigation, a drastic decrease in the average values has been noticed up to the point of separation. The values of average Nusselt numbers have reached their steady-state values at around $\tau = 10.0$. Average Nusselt numbers are found to be higher for smaller pitch to diameter ratios and vice versa.

5.5. *Pressure coefficient*

The pressure coefficient is defined as

$$C_p = 2(P - P_{in}). \tag{7}$$

Fig. 6 shows the pressure distribution along CD of the computational domain. The pressure drop across the first row of cylinders is almost identical with the one over the front of a single cylinder and remains unchanged even after the flow reaches steady state. This holds good for both the PDRs under investigation. From the second row onwards, the pressure drop and recovery are time dependent. It can be seen from the plot that, before the flow stabilizes, the pressure distribution temporarily oscillates with time. It is conjectured that this minor oscillation is due to the eddy size passing through a temporary maximum before reaching steady state. Another observation is that the length of the recirculation zone behind the

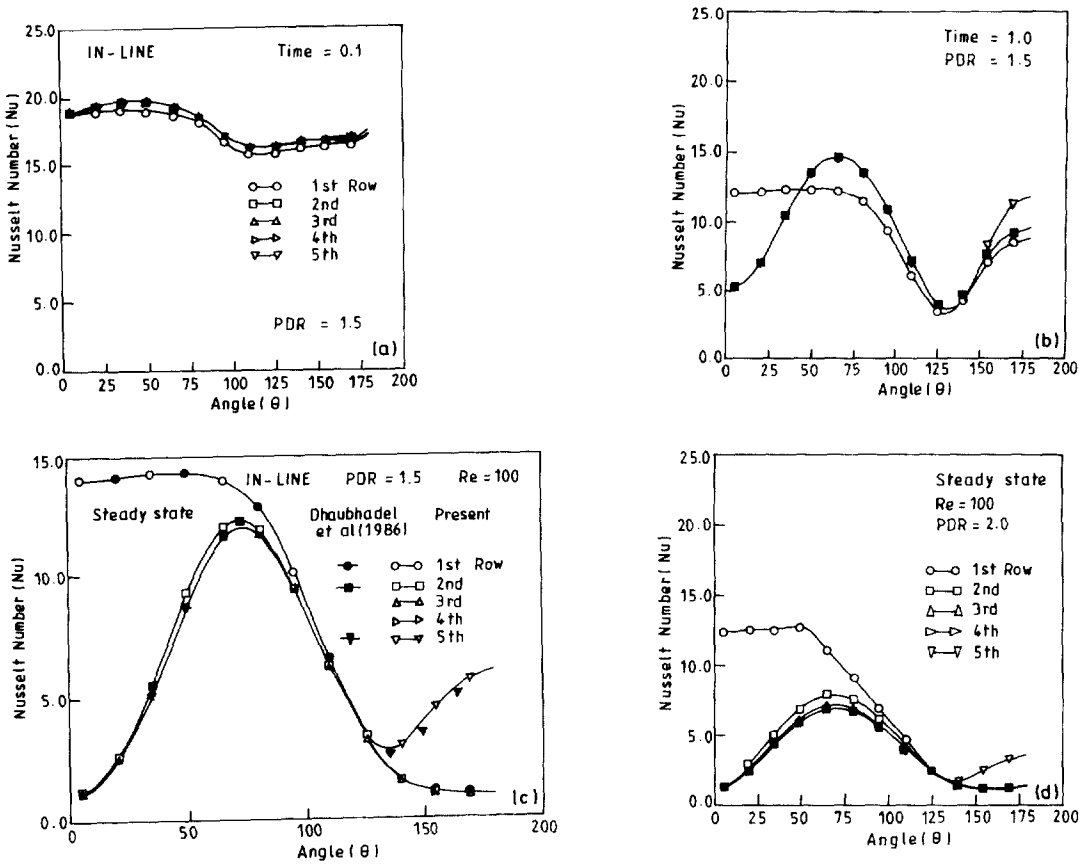

Fig. 5. Distribution of local Nusselt number: PDR = 1.5 and 2.0.

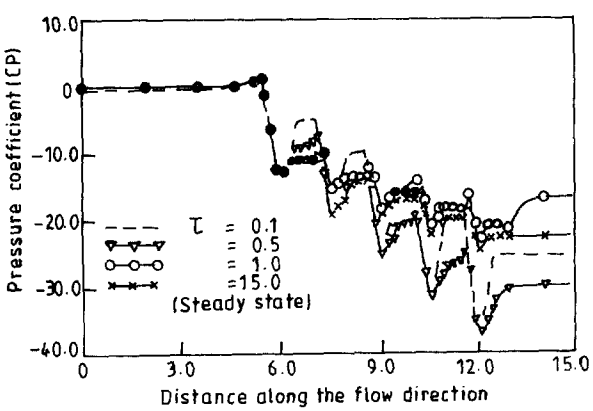

Fig. 6. Pressure distribution around cylinders for PDR = 1.5.

fifth row of cylinders has an influence on the pressure drop and recovery. Furthermore, the pressure drop across the tube bank with PDR = 2.0 is lower (when compared to PDR = 1.5), which is physically consistent with the flow field.

6. Summary and conclusions

Transient fluid flow and heat transfer past an in-line tube bank is numerically simulated by two schemes; namely explicit and semi-implicit. A Reynolds number of 100, Prandtl number of 0.7, and PDRs of 1.5 and 2.0 are chosen for the investigation. The main results of the present investigation are summarized as follows.

- A comparison of two schemes, namely, explicit and semi-implicit has been carried out, which indicated a reduction in the CPU time for the semi-implicit scheme.
- Numerical flow visuals are drawn with respect to time, which depict the eddy growth in the recirculating regions and its subsequent steady state behavior.
- The variation of the Nusselt number with time is rapid during starting phase of the heat exchange between the cylinders and the fluid, as for the average friction coefficient.
- The rates of decrease in the values of average Nusselt numbers and the average friction coefficients are found to be dependent on PDRs and are higher for smaller PDRs and vice versa.
- A higher pressure drop across the bank is seen for PDR of 1.5 than for PDR = 2.0.

References

Braun, M.J., Kudriavtsev, V.V., 1995. Fluid flow structures in staggered bank of cylinders located in a channel. Trans. ASME 117, 36–44.

Collins, R.J., 1973. Band width reduction by automatic renumbering. Int. J. Numer. Meth. Eng. 6, 345–356.

Dhaubhadel, M.N., Reddy, J.N., Telionis, D.P., 1986. Penalty finite-element analysis of coupled fluid flow and heat transfer for in-line bundle of cylinders in cross flow. J. Nonlinear Mech. 21, 361–373.

Donea, J.S., Giuliani, S., Lavel, H., 1982. Finite element solution of unsteady Navier–Stokes equations by fractional step method. Comp. Meth. Appl. Mech. Eng. 30, 53–73.

Franz, Z., Fletcher, C.A., Behnia, M., 1995. Numerical laminar and turbulent fluid flow and heat transfer predictions in tube banks. Int. J. Numer. Meth. Heat Fluid Flow 5, 717–733.

Fujii, M., Fujii, T., Nagata, T., 1984. A numerical analysis of laminar flow and heat transfer of air to in-line tube bank. Numer. Heat Transfer 7, 89–102.

Krishne Gowda, Y.T., 1996. Finite element simulation of flow past tube banks with heat transfer. Ph.D. thesis, IIT, Madras, India.

Launder, B.E., Massey, T.H., 1978. The numerical predictions of viscous flow and heat transfer in tube banks. J. Heat Transfer 100, 565–571.

Patnaik, B.S.V.P., Seetharamu, K.N., Narayana, P.A.A., 1996. Simulation of laminar confined flow past a circular cylinder with integral wake splitter involving heat transfer. Int. J. Numer. Meth. Heat Fluid Flow 6, 65–81.

Ramaswamy, B., Jue, T.C., Akin, J.F., 1992. Semi-implicit and explicit finite element schemes for coupled fluid/thermal problems. Int. J. Numer. Meth. Eng. 34, 675–696.

Wung, T.-S., Chen, C.J., 1989. Finite analytic solution of convective heat transfer for tube arrays in cross flow. J. Heat Transfer 111, 633–640.

Zukauskas, A., 1987. Heat transfer from tubes in cross flow. Adv. Heat Transfer 18, 87–157.